Differential effects of anesthetics on resting state functional connectivity in the mouse

Hongyu Xie[1,2,*], David Y Chung[1,3,*] , Sreekanth Kura[4],
Kazutaka Sugimoto[1,5] , Sanem A Aykan[1], Yi Wu[2],
Sava Sakadžić[6], Mohammad A Yaseen[6], David A Boas[4,6]
and Cenk Ayata[1,7]

Abstract

Blood oxygen level-dependent (BOLD) functional MRI (fMRI) is a standard approach to examine resting state functional connectivity (RSFC), but fMRI in animal models is challenging. Recently, functional optical intrinsic signal imaging—which relies on the same hemodynamic signal underlying BOLD fMRI—has been developed as a complementary approach to assess RSFC in mice. Since it is difficult to ensure that an animal is in a truly resting state while awake, RSFC measurements under anesthesia remain an important approach. Therefore, we systematically examined measures of RSFC using non-invasive, widefield optical intrinsic signal imaging under five different anesthetics in male C57BL/6J mice. We find excellent seed-based, global, and interhemispheric connectivity using tribromoethanol (Avertin) and ketamine–xylazine, comparable to results in the literature including awake animals. Urethane anesthesia yielded intermediate results, while chloral hydrate and isoflurane were both associated with poor RSFC. Furthermore, we found a correspondence between the strength of RSFC and the power of low-frequency hemodynamic fluctuations. In conclusion, Avertin and ketamine–xylazine provide robust and reproducible measures of RSFC in mice, whereas chloral hydrate and isoflurane do not.

Introduction

What determines normal human cognition, and its disorders, is a fundamental question in neuroscience. One approach which has provided insight into the pathophysiology of cognitive disorders is assessment of resting state functional connectivity (RSFC) using, for example, fMRI, PET, and magnetoencephalography.[1,2] However, some questions regarding the pathophysiology of cognition can only be answered with use of experimental models. Practical animal models to assess functional connectivity can help dissect causality, particularly in mice where disease models can be created. Mouse models are also amenable to transgenic approaches where cellular or chemical determinants can be manipulated. Unfortunately, imaging modalities used in humans such as fMRI are challenging in the mouse due to low spatial resolution, limited availability, and

[1]Neurovascular Research Laboratory, Department of Radiology, Massachusetts General Hospital, Charlestown, MA, USA
[2]Department of Rehabilitation, Huashan Hospital, Fudan University, Shanghai, China
[3]Division of Neurocritical Care, Department of Neurology, Massachusetts General Hospital, Boston, MA, USA
[4]Neurophotonics Center, Department of Biomedical Engineering, Boston University, Boston, MA, USA
[5]Department of Neurosurgery, Yamaguchi University School of Medicine, Ube, Japan
[6]Athinoula A. Martinos Center for Biomedical Imaging, Department of Radiology, Massachusetts General Hospital, Charlestown, MA, USA
[7]Stroke Service, Department of Neurology, Massachusetts General Hospital, Boston, MA, USA

*These authors contributed equally to this work.

Corresponding author:
David Y Chung, Massachusetts General Hospital, 149 13th Street, 6403, Charlestown, MA 02129, USA.
Email: dychung@mgh.harvard.edu

difficulty in maintaining stable physiology within a scanner under anesthesia.[3,4] Non-invasive functional optical intrinsic signal imaging has emerged as an excellent complementary method to assess RSFC in mice, utilizing similar physiological phenomena as BOLD fMRI to capture much of the lissencephalic dorsal cortex with high spatial resolution.[5–7]

More recently, optical imaging in awake mice has gained momentum to minimize potential confounding effects of anesthesia. One study has suggested that the signal-to-noise ratio of the hemodynamic signal used to calculate functional connectivity maps in awake animals is greater than that obtained when anesthesia is used.[8] However, another study showed that the robust awake optical hemodynamic signal is linked to subtle movements that can be detected with pressure sensors and cameras focused on whisker position,[9] raising questions about how to define or determine "resting state" in awake animals. Furthermore, experiments involving acute injury, surgical preparation, or interventions that can result in animal distress cannot be performed in awake animals. Therefore, anesthesia will continue to play an important role in RSFC imaging.

There are many anesthetic choices that differ widely in their mechanisms of action and cerebral hemodynamic effects. However, there are limited data in the literature to guide the choice of the optimal anesthetic for intrinsic signal-based RSFC measurements. We, therefore, examined a range of commonly used anesthetics—tribromoethanol (Avertin), ketamine–xylazine, urethane, chloral hydrate, and isoflurane—to determine their suitability for non-invasive functional optical intrinsic signal imaging of RSFC in mice.

Material and methods

Animals

Experiments were performed in accordance with the Guide for Care and Use of Laboratory Animals (NIH Publication No. 85-23,1996). Compliance with the ARRIVE guidelines for reporting in vivo experiments was confirmed except that randomization to anesthetic was not possible. Protocols were approved by our Institutional Animal Care and Use Committee (MGH Subcommittee on Research Animal Care). C57BL/6J mice (male, Charles River Laboratories, Wilmington, MA, USA) between 10 and 20 weeks of age were used for all experiments.

Anesthesia

All anesthetics were titrated for minimal concentrations and doses to achieve absence of withdrawal response to painful stimuli. *Isoflurane* ($n = 4$ mice; Piramal,

#66794-017-25) was given at a concentration of 4% for induction, 1.5–2% for surgical depth of anesthesia during skull preparation, and 1.0%–1.5% during imaging (in $N_2O:O_2$ mixture at 70:30). *Chloral hydrate* ($n = 5$ mice; 370 mg/kg in 90 mg/ml; Paterson Veterinary Supply), *urethane* ($n = 5$ mice; 1100 mg/kg in 100 mg/ml; Acros, #325540500), *ketamine–xylazine* ($n = 5$ mice; 100 and 5 mg/kg in 20 and 1 mg/ml, respectively; Paterson Veterinary supply), and *2,2,2-tribromoethanol* (Avertin, n=5 mice; 300 mg/kg in 20 mg/ml containing 1.25% tert-amyl alcohol; Sigma-Aldrich, T48402-25G and Fisher Scientific, A730-1, respectively) were administered intraperitoneally. Care was taken to protect all solutions from light.

Imaging

Preparation of the skull for imaging experiments has been previously described.[10,11] In brief, the animal was anesthetized, placed on a homeothermic heating pad set for maintaining the core body temperature at $37.0 \pm 0.1°C$, and head fixed in a stereotaxic frame. The skull was exposed after a midline scalp incision. Mineral oil was applied to the skull surface while clearing it of overlying connective tissue. Care was taken to prevent opacification of the skull by reapplying mineral oil as needed. To simplify the experimental setup and analysis, we used a single 570 nm wavelength for RSFC measurements centered at the isosbestic point between deoxy- and oxyhemoglobin, reflecting changes in total hemoglobin concentration (i.e. blood volume). We have previously described quantitative equivalence between this single wavelength approach and traditional multi-wavelength analysis.[7] The surface of the skull was illuminated by light from a quartz tungsten halogen lamp (Techniquip R150, Capra Optical, Natick, MA) passed through a 570 ± 10 nm filter and directed with a fiber optic cable. Images were acquired with a CCD camera (Cascade 512F, Photometrics) at 256×256 pixel resolution (2×2 binning) and 13.6 frames per second for 10 min. μManager software was used for image acquisition.[12] Animals were euthanized by cervical dislocation immediately following completion of imaging experiments.

Image analysis and RSFC indices

Detailed methods for the processing and generation of the intrinsic signal and functional connectivity correlation coefficients have been described previously.[5,7] In brief, using custom-written scripts in MATLAB (Math Works, Natick, MA, USA), acquired images were downsampled to 128×128 pixels. The optical density at each resulting pixel over the time course of the experiment was calculated. The dynamic optical density

maps were bandpass filtered between 0.008 Hz and 0.09 Hz, downsampled to 1 frame per second, and regressed to remove any global source of signal variance. To generate *seed-based connectivity maps*, seeds were manually placed in motor, somatosensory, retrosplenial, and visual cortex guided by the coordinates of an overlaid atlas by Paxinos and Franklin,[13] and correlation coefficients between the seed and all other pixels were calculated and mapped throughout the image. Seed-to-seed correlation coefficients were also calculated and plotted on a *seed-to-seed connection matrix*. By averaging the positive correlation coefficients between a seed and all other pixels in the map, we calculated a *seed-based connectivity index*. *Global connectivity maps* were generated by finding the correlation coefficient between each pixel and all other pixels, averaging the positive correlation coefficients between a particular pixel and all other pixels, and then displaying the averaged correlation coefficient for that pixel in the map. A *global connectivity index* was then calculated by taking the mean of the correlation coefficients for all pixels within the global connectivity map. *Interhemispheric homotopic connectivity maps* were determined by calculating the correlation coefficient between a pixel and its mirror pixel in contralateral cortex, taking care to mirror pixels in a plane orthogonal to a manually drawn midline. The *interhemispheric homotopic connectivity index* was then calculated by taking the mean of all the pixels within the interhemispheric homotopic connectivity map.

Blood pressure

In imaging experiments, we avoided extensive surgery to minimize potential confounders. Therefore, we measured the mean arterial pressure (MAP), pH, and blood gas values in a separate cohort of mice. Isoflurane and Avertin were chosen as they provided the worst and best measures of functional connectivity.

The mouse was anesthetized with 4% isoflurane (in $N_2O:O_2$ mixture at 70:30) for induction. This was reduced to 1.5-2% for surgical depth of anesthesia during arterial femoral line insertion with PE-10 tubing connected to a pressure transducer. The depth of anesthesia was then reduced further to imaging levels of 1.0%–1.5% and blood pressure was measured over 10 minutes. Avertin was then injected (300 mg/kg) and isoflurane gradually titrated down over 10 min. Blood pressure was measured for another 10 min on Avertin alone. This sequential design was necessary because Avertin did not provide surgical depth of anesthesia to allow femoral artery cannulation. The arterial pressure, pH, and blood gases were all within previously reported normal physiological limits for mice[14] (Supplemental Table).

Statistics

Statistical comparisons were made using one- or two-way repeated-measures ANOVA, Kruskal–Wallis tests, and paired *t*-tests as appropriate (Prism 7, GraphPad Software, Inc., CA, USA), and indicated for each data set in figure legends. SAS (Version 9.4, SAS Institute, Cary, NC) was used to create a multivariable general linear mixed effects model for the seed-based connectivity analysis. Two models with the dependent variable of correlation coefficient were created: (1) seed location, anesthetic, and hemisphere side and (2) seed location and anesthetic. All error bars in figures represent standard deviations unless otherwise specified.

Results

All four seeds showed strong interhemispheric correlations on *seed-based connectivity maps* (Figure 1(a)), consistent with previous reports by us and others.[5–7] Anesthetic choice significantly affected the seed-based connectivity maps. Avertin and ketamine–xylazine consistently yielded stronger connectivity in all four seeds, although Avertin appeared to be marginally superior to ketamine–xylazine. They were followed by urethane, which also yielded conspicuous correlations albeit qualitatively weaker than Avertin and ketamine–xylazine. In contrast, seed-based correlation maps were both qualitatively (Figure 1(a)) and quantitatively (Figure 1(d)) inferior under both chloral hydrate and isoflurane anesthesia, with barely discernible interhemispheric correlations.

The *seed-to-seed connection matrix* reflected the same anesthetic hierarchy (Figure 1(b)). The absolute magnitude of the correlation coefficients between each seed pair was greatest for Avertin and ketamine–xylazine, followed by urethane, and lowest with chloral hydrate and isoflurane. A multivariable general linear mixed effects model accounting for the anesthetic choice and seed pairs in the connection matrix revealed these differences to be highly statistically significant ($p < 0.0001$ for main anesthetic effect; Table 1). Furthermore, the coefficient of variation of the correlation coefficients for urethane, chloral hydrate, and isoflurane was overall greater than the coefficients of variation for Avertin and ketamine–xylazine, suggesting significantly lower signal-to-noise ratios with the latter two anesthetics (Figure 1(c)).

The *seed-based connectivity index*, calculated by averaging the correlation coefficients of all positive pixels within the connectivity map for each seed, reproduced the anesthetic hierarchy (from strongest to weakest: Avertin, ketamine–xylazine, urethane, chloral hydrate, and isoflurane) and additionally revealed that motor and visual cortex seed-based connectivity
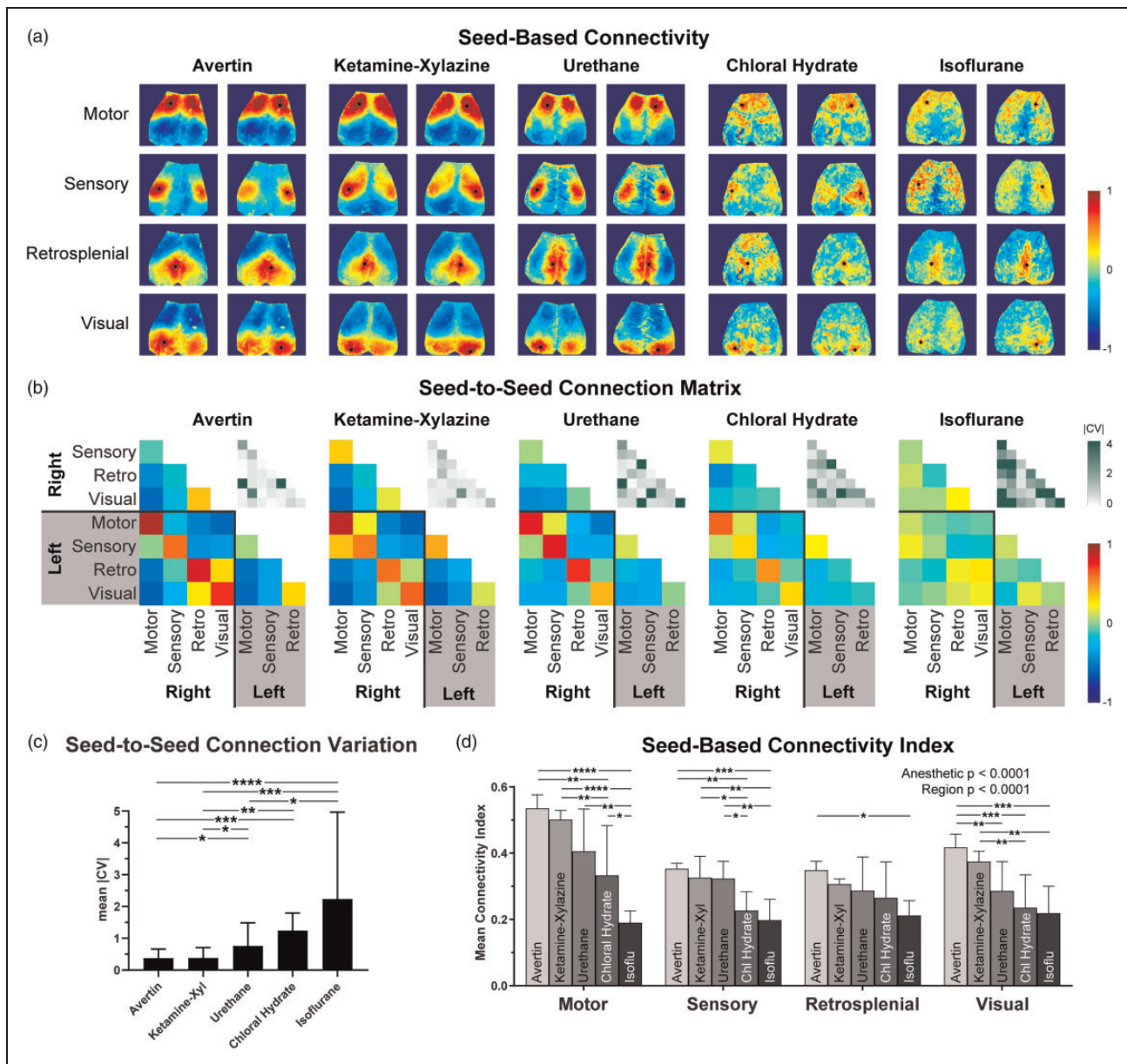
Figure 1. Seed-based connectivity varies based on the anesthetic used. (a) Representative seed-based connectivity maps for Avertin, ketamine–xylazine, urethane, chloral hydrate, and isoflurane. (b) Averaged connection matrices among the eight seeds. The absolute value of the coefficient of variation of the correlation coefficients for each pair in the matrix (|CV|) is shown in the upper right of each panel. (c) Median |CV| for each of the anesthetics tested (error bars are 25–75% interquartile range). (d) Average correlation coefficient of the map for all positive values associated with each seed. The number of mice for each experiment was $n = 5$ for Avertin, $n = 5$ for ketamine–xylazine, $n = 5$ for urethane, $n = 5$ for chloral hydrate, and $n = 4$ for isoflurane. *$p < 0.05$, **$p < 0.01$, ***$p < 0.001$, ****$p < 0.0001$, Bonferroni-corrected for parametric tests and corrected using Dunn's statistical hypothesis testing for non-parametric tests.

indices were more anesthetic-dependent than the sensory and retrosplenial seeds (Figure 1(d)). To statistically test this, we employed a multivariable general linear mixed effects model accounting for the four regions, the hemispheres (right vs. left), and the five anesthetics as independent variables, and seed-based connectivity index as the dependent variable. Since

the hemisphere did not significantly influence the seed-based connectivity index ($p = 0.46$), we removed this variable from the model. We found that both anesthetic and cortical region had significant main effects on the seed-based connectivity index (both with $p < 0.0001$). Post hoc comparisons revealed significant differences between anesthetics in motor, sensory,

Table 1. Seed-to-seed connection matrix p-values (Bonferroni-corrected for multiple comparisons) for Figure 1(b).

	Avertin	Ketamine–xylazine	Urethane	Chloral hydrate
Ketamine–Xyl	*0.90*			
Urethane	**0.0003**	**0.0003**		
Chloral hydrate	**<0.0001**	**<0.0001**	*0.071*	
Isoflurane	**<0.0001**	**<0.0001**	**<0.0001**	**0.0046**

Note: Bold indicates statistically significant differences and italics indicate non-significant differences.

Table 2. Seed-based connectivity index comparisons p-values (Bonferroni-corrected for multiple comparisons) for Figure 1(d).

	Avertin	Ketamine–xylazine	Urethane	Chloral hydrate
Ketamine–Xyl	*0.58*			
Urethane	**0.0011**	*0.10*		
Chloral hydrate	**<0.0001**	**<0.0001**	**0.035**	
Isoflurane	**<0.0001**	**<0.0001**	**<0.0001**	*0.052*

visual, and, to a lesser extent, retrosplenial seeds as indicated in Figure 1(d). When all seeds were pooled, every anesthetic was significantly different from each other ($p < 0.05$ with Bonferroni correction for multiple comparisons) except for Avertin vs. ketamine–xylazine ($p = 0.58$), ketamine–xylazine vs. urethane ($p = 0.10$), and choral hydrate vs. isoflurane ($p = 0.052$) (Table 2).

To assess a seed-independent index of RSFC, we generated *global connectivity maps* and calculated *global connectivity indices* for each anesthetic (Figure 2). Qualitatively, global connectivity maps showed the strongest connectivity in both Avertin and ketamine–xylazine groups, and weakest connectivity under chloral hydrate or isoflurane anesthesia (Figure 2(a)). The quantitative global connectivity index significantly differed among the anesthetics ($p = 0.0010$, one-way ANOVA; Figure 2(b)). The cumulative correlation coefficient histograms showed that almost all pixels were below a global connectivity index of 0.3 in chloral hydrate and isoflurane groups, whereas 50% of pixels were above this cutoff under Avertin, ketamine–xylazine and urethane anesthesia (Figure 2(c)). The mean global connectivity indices obtained from the Gaussian fit of the histogram reproduced the mean global connectivity indices of all pixels (not shown).

To selectively interrogate interhemispheric connectivity, we created *interhemispheric homotopic connectivity maps* and calculated *interhemispheric homotopic connectivity indices* between "mirror" pixels based on midline symmetry. Interhemispheric homotopic connectivity maps typically yielded much stronger

correlation coefficients compared with global connectivity maps. Interhemispheric connectivity maps were similar among Avertin, ketamine–xylazine, and urethane anesthesia, all of which were distinctly stronger than chloral hydrate and isoflurane (Figure 2(d)). The interhemispheric connectivity index significantly differed among the anesthetics ($p = 0.0004$, one-way ANOVA) and reproduced the same hierarchy observed with seed-based and global connectivity indices albeit with greater separations among the anesthetics (Figure 2(e)). The cumulative correlation coefficient histograms favored Avertin over ketamine–xylazine and urethane; 60% of all pixels had an interhemispheric homotopic correlation coefficient of 0.6 or higher under Avertin anesthesia (Figure 2(f)). The mean interhemispheric homotopic connectivity indices obtained from the Gaussian fit of the histogram reproduced the mean interhemispheric homotopic connectivity indices of all pixels (not shown).

To gain insight into the physiological substrates of anesthetic modulation of RSFC, we examined the global signal-regressed intrinsic signal changes during each imaging session under each of the five anesthetics. We noted large amplitude hemodynamic fluctuations of total hemoglobin (i.e. cerebral blood volume) under Avertin anesthesia (Supplemental Movie). Urethane and ketamine–xylazine showed smaller amplitude fluctuations, whereas chloral hydrate and isoflurane groups were completely flat (Supplemental Movie). These hemodynamic fluctuations were highly symmetric between the hemispheres and emerged as stereotypic regional hyperemic transients (Figure 3(a)), at times approximating seed-based connectivity maps (Figure 1(a)). They appeared in no particular order, and were likely the primary drivers of the RSFC in cortex, at least under our experimental conditions. To represent the dynamic nature of these regional hyperemic transients, we selected a sagittal line-of-interest (LOI) across motor, somatosensory and visual cortices (Figure 3(a) and (b) dashed line) in representative mice under Avertin and isoflurane. We plotted the magnitude of the hemodynamic signal as a function of time for the entire imaging session (Figure 3(a) and (b)). This LOI time course revealed discrete state changes of variable durations under Avertin anesthesia, which were completely absent under isoflurane. To quantify this finding for all anesthetics, we calculated the power of hemodynamic signal fluctuations at each pixel and generated a power map (Figure 3(c)). The mean power, calculated by averaging pixel power throughout each map, differed by more than an order of magnitude between the highest (Avertin) and lowest (isoflurane) power group (Figure 3(d)), and correlated well with the mean power calculated using just the LOIs (Figure 3(e)). Interestingly, ketamine–xylazine showed
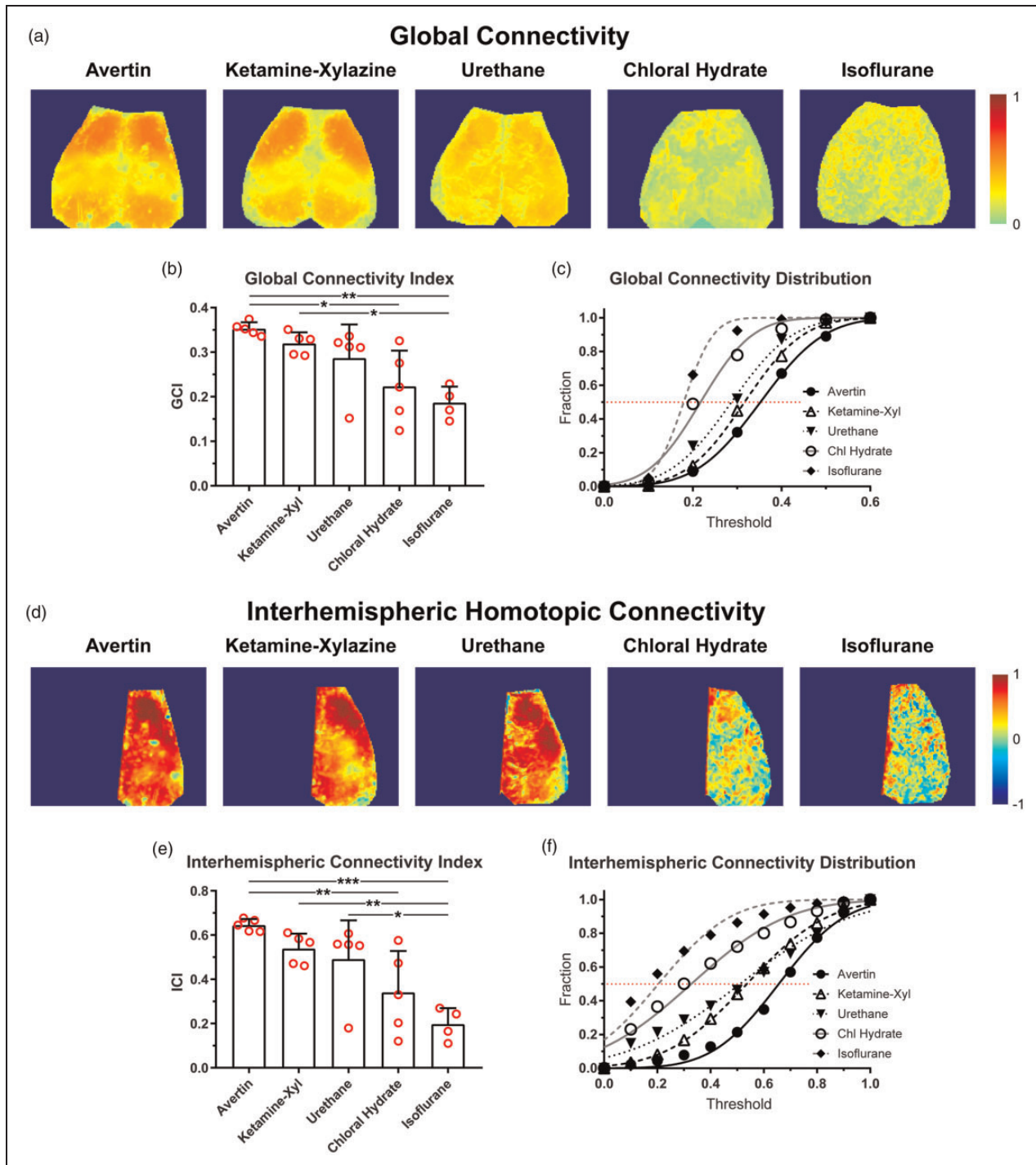
Figure 2. Global and interhemispheric homotopic connectivity varies based on the anesthetic used. (a) Representative maps showing the mean correlation coefficient of each pixel to every other pixel within the map for Avertin, ketamine–xylazine, urethane, chloral hydrate, and isoflurane. Only positive correlations were used for the maps. (b) A global connectivity index (GCI) was calculated which took the means of all the pixels within the maps from (a) for each anesthetic. (c) The proportion of pixels below a threshold mean correlation coefficient is plotted and fitted with a Gaussian distribution. (d) Representative maps showing the correlation coefficient of a pixel in one hemisphere with its mirror pixel in contralateral hemisphere (i.e. its homotopic partner in contralateral hemisphere). (e) An interhemispheric connectivity index (ICI) was calculated which took the means of all the pixels within the maps from (d) for each anesthetic. (f) The proportion of pixels below a threshold mean correlation coefficient is plotted and fitted with a Gaussian distribution. *$p < 0.05$, **$p < 0.01$, ***$p < 0.001$, Bonferroni-corrected.
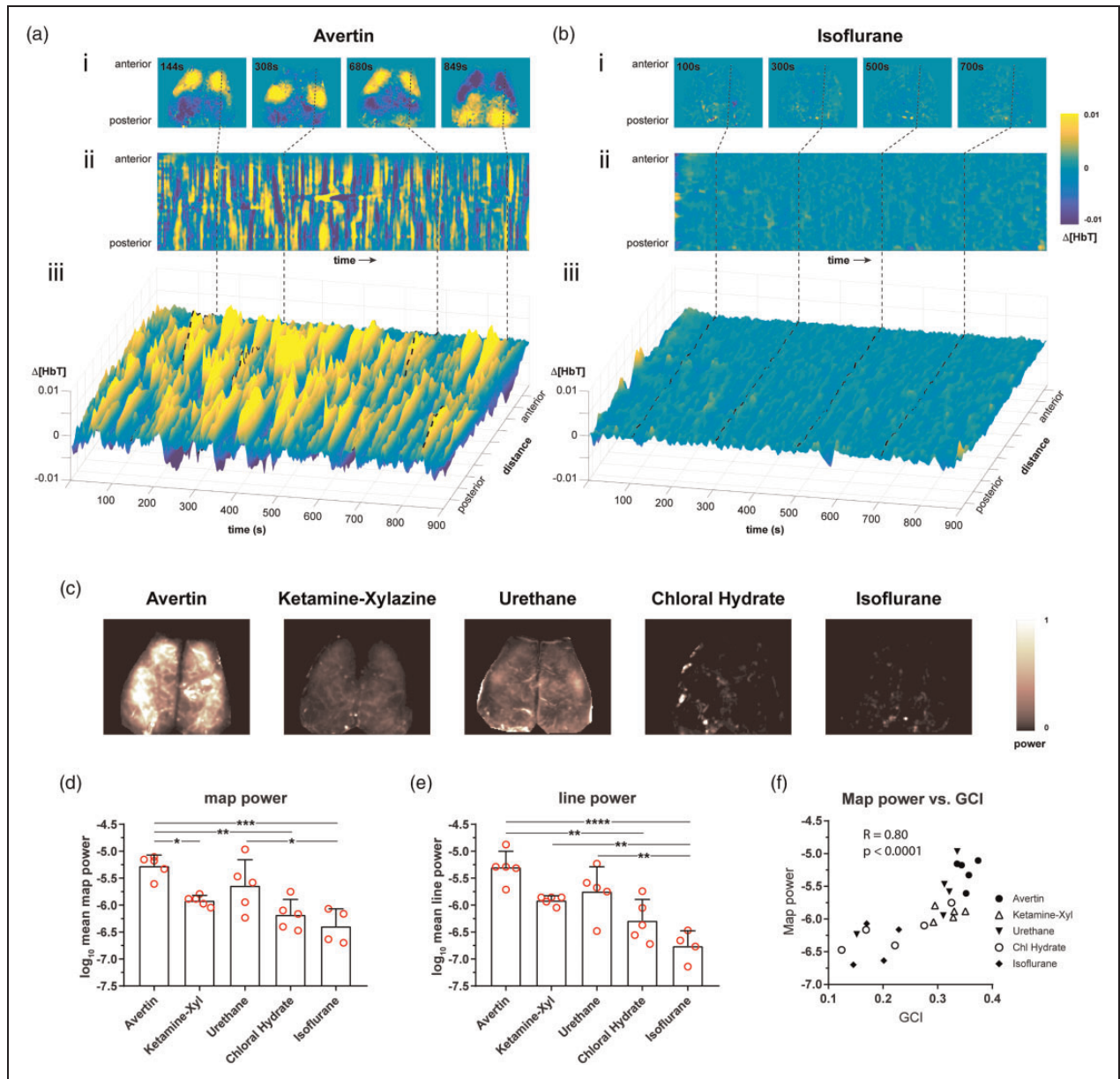
Figure 3. Anesthetics have differential effects on the amplitude of the globally regressed, low-frequency hemodynamic signal. (a and b) Avertin and isoflurane were chosen as examples to demonstrate the differences in the spatiotemporal fluctuations in the hemodynamic signal. (i) Representative maps at different time points during an imaging session show relative common patterns of blood volume distribution across the dorsal surface of brain. (ii) A sagittal profile was drawn through the motor, somatosensory, and visual cortices (dashed line), and the hemodynamic signal across the line was plotted over of time. (iii) A three-dimensional representation of (ii) is shown to highlight regional changes in blood volume fluctuations and the difference in the hemodynamic signal between Avertin and isoflurane. (c) Representative power maps show the amplitude of the hemodynamic fluctuations used to derive functional connectivity for Avertin, ketamine–xylazine, urethane, chloral hydrate, and isoflurane. Power is normalized between 0 and 1 in the scale. (d) The average power for all pixels in the hemodynamic map for each anesthetic is shown. (e) The average power along the sagittal profile drawn over the hemodynamic map for each anesthetic is shown. (f) Power of the hemodynamic signal correlates with the GCI (global connectivity index) across anesthetics. R is the Pearson correlation coefficient. $*p < 0.05$, $**p < 0.01$, $***p < 0.001$, $****p < 0.0001$, Bonferroni-corrected.

somewhat lower mean power than urethane, even though it usually yielded higher correlation coefficients. Nevertheless, mean power of the hemodynamic signal correlated strongly with the global connectivity index across all animals and anesthetics (Figure 3(f)).

Discussion

Our data indicate that the choice of anesthetic dramatically influences all indices of RSFC including the magnitude of the underlying hemodynamic signal. Avertin gives the most robust signal under our experimental conditions, followed closely by ketamine–xylazine. Urethane provides reasonable RSFC output as well. However, chloral hydrate and isoflurane are not suitable for use as anesthetics under our experimental conditions.

The need for a practical way to measure RSFC in mice was addressed by White et al.[5] who established key measures of functional connectivity using optical intrinsic signal imaging through intact mouse skull.[5] This approach has been subsequently reproduced by other groups under both awake and anesthetized conditions[6,7,15,16] and has offered the promise to investigate long-range network activity in the setting of pathologies such as Alzheimer's disease and ischemic stroke.[17,18] However, recent work has suggested that the resting state hemodynamic signal can be adversely affected by the presence of anesthesia as compared to the awake mouse.[8] Furthermore, an exquisitely detailed study in awake mice performed by Winder et al.[9] that took advantage of multiple movement sensors has suggested that it is potentially very difficult to get true awake resting state data that is not contaminated by subtle movements. The study also found that when true awake resting state imaging was achieved, the signal-to-noise ratio of their optical density recordings was very low. These data imply that movement poses a considerable confound for awake RSFC imaging, limiting the technique's robustness and adoption by the scientific community. Therefore, until these confounds can be suitably addressed, we believe there is an important role for RSFC experiments conducted under anesthesia.

As there has not been a systematic study evaluating the effect of different commonly used anesthetics on RSFC in mice, we tested the effects of Avertin, ketamine–xylazine, urethane, chloral hydrate, and isoflurane on multiple connectivity measures. Our RSFC maps were consistent with prior studies under a ketamine (an NMDA receptor antagonist) and xylazine combination,[5,16–19] and our hemodynamic fluctuation maps were similar to a prior study under urethane.[8] The RSFC maps for Avertin, ketamine–xylazine, and urethane were also consistent with awake imaging studies.[6,15,16] Chloral hydrate and isoflurane were not

suitable for RSFC imaging, likely due to the severely attenuated low-frequency hemodynamic signal (Figure 3). The reasons for this are unclear. We tested chloral hydrate because of its reputation as a light anesthetic,[20] but found that at the doses needed to provide adequate anesthesia (i.e. absence of withdrawal response to painful stimuli) the hemodynamic signal was nearly abolished. We observed the same with isoflurane, which was surprising considering the fact that isoflurane is widely used for resting state fMRI in the mouse apparently with good results,[21,22] and that our optical signal is similar to the BOLD signal. The discrepancy may be related to our selection of wavelength mainly sensitive to blood volume changes, whereas the BOLD signal may in part reflect hemoglobin oxygenation changes.[4,23] Notably, there is a report of good quality RSFC measurements using lower doses of isoflurane (0.5–0.8%),[24] but we were not able to prevent movement artifact with these doses under our experimental conditions.

We did not attempt to elucidate the mechanisms underlying the differential effects of tested anesthetics on RSFC. One mechanism may relate to resting cerebrovascular tone and vasomotor reactivity. We have previously shown using wide-field laser speckle flowmetry that isoflurane anesthesia is associated with a two-fold higher resting cerebral blood flow (CBF) compared with α-chloralose,[25] similar to chloral hydrate used herein, and may lead to maximal vasodilation diminishing spontaneous hemodynamic fluctuations (i.e. ceiling effect). Moreover, α-chloralose anesthesia is known preserve cerebral vasomotor responses (e.g. hypercapnic hyperemia, autoregulation), whereas isoflurane disrupts them.[26] Yet, both isoflurane and chloral hydrate yielded the weakest RSFC indices in our study, suggesting that resting state CBF and vasoreactivity alone cannot explain the anesthetic-related differences in RSFC indices. Arterial blood pressure, pCO_2 and pH can also vary under different anesthetics. We observed higher pCO_2, and lower pH and blood pressure under Avertin anesthesia compared with isoflurane, which may lead to reduced cerebrovascular tone and diminished spontaneous hemodynamic fluctuations. Yet, Avertin yielded the best RSFC indices among all anesthetics, suggesting that systemic physiological values within the ranges observed in our study also did not significantly affect the RSFC signal. Additional studies are needed to determine the mechanisms of anesthetic effects on RSFC.

Our study has limitations. First, we used the hemodynamic signal as a surrogate for underlying neuronal activity, and, therefore, our interpretation is susceptible to confounding effects of neurovascular uncoupling. This may in part explain the poor yield under isoflurane. Furthermore, there may be regional variations in

the hemodynamic response.[19] Nevertheless, RSFC based on direct imaging of neuronal activity requires transgenic models expressing fluorescent indicators,[8,27] which is a limitation in itself. Second, we do not have a quantitative measure of anesthetic depth. A universal, objective parametric indicator of the depth of anesthesia does not yet exist. Therefore, we used the minimum amount of anesthesia required to abolish the reflex movements to painful stimuli during the imaging. Lower doses of anesthesia that may be considered acceptable in the absence of acute surgical interventions used herein may yield better RSFC. Third, we only used male mice for the study. Future studies should include both male and female mice. Finally, there are many other anesthetics potentially applicable to RSFC. We tried to pick five anesthetic regimens with diverse mechanisms of action to the extent that they are known, and anticipate that anesthetics which belong to the same class will yield similar outcomes.

Based on our data, some recommendations can be made for the optimal choice of anesthetic in optical RSFC imaging. In our hands, Avertin consistently yielded the best results overall in multiple indices of RSFC and the magnitude of the hemodynamic signal. Ketamine–xylazine also gave excellent results and may be favored in some translational studies given the availability of ketamine for clinical use. Urethane can be convenient; however, experiments are terminal as mice do not recover from urethane anesthesia, it is potentially carcinogenic,[28] and it had the highest coefficient of variation (i.e. signal to noise) of useable anesthetics in our study. Chloral hydrate and isoflurane are not suitable for RSFC optical imaging in mice, at least when using the single isosbestic wavelength of light at a surgical depth of anesthesia.

Conclusions

Our data show that anesthetics markedly influence multiple RSFC indices, underlying hemodynamic signals, and measures of signal-to-noise. Avertin emerged as the best anesthetic tested, while ketamine–xylazine also yielded excellent results. Urethane provided acceptable results. Chloral hydrate and isoflurane were not suitable under our experimental conditions. Altogether, our data underscore the importance of choice of anesthesia on measures of RSFC by optical imaging, or fMRI, and serve as a reference point for future studies.

Funding

Declaration of conflicting interests

Authors' contributions

HX contributed to the concept and design of the study and acquisition of data. DYC contributed to the acquisition, analysis, and interpretation of data, and drafted the article. SK contributed to the analysis and interpretation of data. KS contributed to acquisition, analysis, and interpretation of data. SAA contributed to acquisition, analysis, and interpretation of data. SS contributed to the analysis and interpretation of data. MAY contributed to the analysis and interpretation of data. DAB contributed to the concept and design of the study. CA contributed to the concept and design of the study, analysis and interpretation of data, and drafted the manuscript. HX, DYC, SK, KS, SAA, YW, SS, MAY, DAB, and CA revised the article critically for important intellectual content and approved the version to be published.

ORCID iDs

David Y Chung (iD) http://orcid.org/0000-0002-7149-5851
Kazutaka Sugimoto (iD) http://orcid.org/0000-0002-7666-2620

Supplemental material

Supplemental material for this paper can be found at the journal website: http://journals.sagepub.com/home/jcb

References

1. Greicius MD, Srivastava G, Reiss AL, et al. Default-mode network activity distinguishes Alzheimer's disease from healthy aging: evidence from functional MRI. *Proc Natl Acad Sci U S A* 2004; 101: 4637–4642.
2. Bassett DS and Sporns O. Network neuroscience. *Nat Neurosci* 2017; 20: 353–364.
3. Pan WJ, Billings JC, Grooms JK, et al. Considerations for resting state functional MRI and functional connectivity studies in rodents. *Front Neurosci* 2015; 9: 269.
4. Desjardins M, Kılıç K, Thunemann M, et al. Awake mouse imaging: from 2-photon microscopy to BOLD fMRI. *Biol Psychiatry Cogn Neurosci Neuroimaging*. Epub ahead of print 12 December 2018. DOI: 10.1016/j.bpsc.2018.12.002.

5. White BR, Bauer AQ, Snyder AZ, et al. Imaging of functional connectivity in the mouse brain. *PloS one* 2011; 6: e16322.

6. Murphy TH, Boyd JD, Bolanos F, et al. High-throughput automated home-cage mesoscopic functional imaging of mouse cortex. *Nat Commun* 2016; 7: 11611.

7. Kura S, Xie H, Fu B, et al. Intrinsic optical signal imaging of the blood volume changes is sufficient for mapping the resting state functional connectivity in the rodent cortex. *J Neural Eng*. Epub ahead of print 16 February 2018. DOI: 10.1088/1741-2552/aaafe4.

8. Ma Y, Shaik MA, Kozberg MG, et al. Resting-state hemodynamics are spatiotemporally coupled to synchronized and symmetric neural activity in excitatory neurons. *Proc Natl Acad Sci U S A* 2016; 113: E8463–E8471.

9. Winder AT, Echagarruga C, Zhang Q, et al. Weak correlations between hemodynamic signals and ongoing neural activity during the resting state. *Nat Neurosci* 2017; 20: 1761–1769.

10. Chung DY, Sadeghian H, Qin T, et al. Determinants of optogenetic cortical spreading depolarizations. *Cereb Cortex* 2019; 29(3): 1150–1161.

11. Chung DY, Sugimoto K, Fischer P, et al. Real-time non-invasive in vivo visible light detection of cortical spreading depolarizations in mice. *J Neurosci Meth* 2018; 309: 143–146.

12. Edelstein AD, Tsuchida MA, Amodaj N, et al. Advanced methods of microscope control using muManager software. *J Biol Methods* 2014; 1(2): pii: e10. DOI: 10.14440/jbm.2014.36.

13. Paxinos G and Franklin KBJ. *The mouse brain in stereotaxic coordinates*. 2nd ed. San Diego: Academic Press, 2001, p.xxv, 132 tav.

14. Dalkara T, Irikura K, Huang Z, et al. Cerebrovascular responses under controlled and monitored physiological conditions in the anesthetized mouse. *J Cereb Blood Flow Metab* 1995; 15: 631–638.

15. Yoshida Y, Nakao M and Katayama N. Resting-state functional connectivity analysis of the mouse brain using intrinsic optical signal imaging of cerebral blood volume dynamics. *Physiol Meas* 2018; 39: 054003.

16. Wright PW, Brier LM, Bauer AQ, et al. Functional connectivity structure of cortical calcium dynamics in anesthetized and awake mice. *PLoS One* 2017; 12: e0185759.

17. Bauer AQ, Kraft AW, Wright PW, et al. Optical imaging of disrupted functional connectivity following ischemic stroke in mice. *Neuroimage* 2014; 99: 388–401.

18. Bero AW, Bauer AQ, Stewart FR, et al. Bidirectional relationship between functional connectivity and amyloid-beta deposition in mouse brain. *J Neurosci* 2012; 32: 4334–4340.

19. Murphy MC, Chan KC, Kim SG, et al. Macroscale variation in resting-state neuronal activity and connectivity assessed by simultaneous calcium imaging, hemodynamic imaging and electrophysiology. *Neuroimage* 2018; 169: 352–362.

20. Field KJ, White WJ and Lang CM. Anaesthetic effects of chloral hydrate, pentobarbitone and urethane in adult male rats. *Lab Anim* 1993; 27: 258–269.

21. Bukhari Q, Schroeter A, Cole DM, et al. Resting state fMRI in mice reveals anesthesia specific signatures of brain functional networks and their interactions. *Front Neural Circuits* 2017; 11: 5.

22. Grandjean J, Schroeter A, Batata I, et al. Optimization of anesthesia protocol for resting-state fMRI in mice based on differential effects of anesthetics on functional connectivity patterns. *Neuroimage* 2014; 102(Pt 2): 838–847.

23. Hillman EM. Coupling mechanism and significance of the BOLD signal: a status report. *Ann Rev Neurosci* 2014; 37: 161–181.

24. Matsui T, Murakami T and Ohki K. Transient neuronal coactivations embedded in globally propagating waves underlie resting-state functional connectivity. *Proc Natl Acad Sci U S A* 2016; 113: 6556–6561.

25. Shin HK, Jones PB, Garcia-Alloza M, et al. Age-dependent cerebrovascular dysfunction in a transgenic mouse model of cerebral amyloid angiopathy. *Brain* 2007; 130: 2310–2319.

26. Ayata C, Dunn AK, Gursoy OY, et al. Laser speckle flowmetry for the study of cerebrovascular physiology in normal and ischemic mouse cortex. *J Cereb Blood Flow Metab* 2004; 24: 744–755.

27. Ma Y, Shaik MA, Kim SH, et al. Wide-field optical mapping of neural activity and brain haemodynamics: considerations and novel approaches. *Philos Trans R Soc Lond B Biol Sci* 2016; 371(1705): pii: 20150360. DOI: 10.1098/rstb.2015.0360.

28. Field KJ and Lang CM. Hazards of urethane (ethyl carbamate): a review of the literature. *Lab Anim* 1988; 22: 255–262.